Induction of Helical Structure in a Heptapeptide with a Metal Cross-Link: Modification of the Lifson−Roig Helix−Coil Theory to Account for Covalent Cross-Links†

Kenneth J. Kise, Jr. and Bruce E. Bowler*

Department of Chemistry and Biochemistry, University of Denver, 2190 East Iliff Avenue, Denver, Colorado 80208-2436

Received August 9, 2002; Revised Manuscript Received November 1, 2002

ABSTRACT: A short peptide, acetyl-AHAAAHA-carboxamide, has been synthesized and the histidines cross-linked with a *cis*-tetraammineruthenium(III) moiety. In the absence of the Ru(III) cross-link, the heptapeptide is essentially structureless, as judged by circular dichroism, NMR chemical shift, and NMR-monitored hydrogen deuterium exchange data. The presence of the *cis*-Ru(III) cross-link is confirmed by mass spectral data and the characteristic pH dependence of the UV−vis spectrum of the *cis*-(bis-(imidazole))ruthenium-(III) unit. Circular dichroism data indicate that the Ru(III) cross-linked heptapeptide is approximately 37% helical at 0 °C. The NMR spectrum of the cross-linked peptide has been fully assigned using TOCSY and ROESY experiments. ROE interactions and *J*-coupling data provide evidence for helical structure. NMR-monitored hydrogen−deuterium exchange data for the Ru(III)-cross-linked peptide, resolved at the level of the individual amides, give larger protection factors at the ends than in the center of the helix. Steric and polarization effects of the Ru(III) cross-link are proposed to cause this unusual apparent protection pattern. A modification to the Lifson−Roig helix−coil model to account for the effect of the *i*,*i*+4 Ru-(III) cross-link on the helix−coil transition of a peptide is presented. The model provides an excellent fit to the temperature dependence of the circular dichroism spectrum of the Ru(III)-cross-linked peptide. The modified model indicates that the effect of the cross-link on the nucleation parameter, v^2, is modest (about 7-fold) for residues bounded by the cross-link. Significant increases in the propagation parameter, *w*, occur for residues within the cross-link. The modification to the Lifson−Roig model accounts for the effect of a Ru(III) cross-link on the circular dichroism spectrum of a previously reported 17 residue peptide.

There is substantial evidence that protein secondary structure forms early in protein folding (*1*−*3*). In fact, a commonly invoked protein folding intermediate, the molten globule (*4*), is characterized by significant secondary structure but little tertiary structure. Given the apparent importance of secondary structure formation early in protein folding, much effort has been directed at understanding the factors that stabilize secondary structure. Strong progress has been made in understanding α-helix formation using alanine-based peptides (*5*). More recently a number of stable peptide models for β-sheet structure have also been developed (*6*). The alanine-based peptides have been of great importance in understanding the intrinsic helix propensities of the individual amino acids (*7*), as well as, the role of side chain−side chain interactions in stabilizing helices (*8*−*10*).

In helix−coil theory, nucleation of helical structure is entropically unfavorable and thus of low probability (*11*−*13*). Once nucleated, the greater favorability of propagation leads to the observed cooperativity of the helix−coil transition and the tendency of individual helical segments to be long. Thus, in general very short peptides do not form any persistent helical structure. Typically peptides in the range of 5−7 amino acids in length have been used to model the properties of a random coil (*14*, *15*). Given the difficulty of nucleation, a number of strategies aimed at enhancing nucleation have been developed in order to stabilize peptide helices. These have normally involved some sort of *i*,*i*+4 chemical cross-link to bias the conformational distribution toward the required *i*,*i*+4 loop. Disulfide bonds (*16*, *17*), bridging Asp−Lys amide cross-links (*18*−*20*) and metal cross-links (*21*−*23*) have all been used successfully. Rigid organic scaffolds have also been developed (*24*, *25*), and the calcium binding loop of calmodulin has been used as a helix nucleator (*26*).

With few exceptions (*19*), cross-links have only been used to stabilize moderate-sized peptides, 15−25 amino acids in length. To obtain a detailed understanding of the effects of such cross-links on nucleation, it is useful to study an isolated helix nucleus in the absence of propagating amino acids. In the work presented here, we have prepared a short seven amino acid peptide, Ac-AHAAAHA-$CONH_2$ (Ac indicates an acetylated N-terminal amino group, $CONH_2$ indicates a C-terminal carboxamide)[1] and studied the effect of a substitution inert metal cross-link between the two histidine side chains spaced *i*,*i*+4, on the structural properties of this peptide. The *cis*-Ru(III)tetraammine cross-link was chosen

† Acknowledgment is made to the donors of the Petroleum Research Fund, administered by the American Chemical Society, for partial support of this work. The Biomolecular Structure and Magnetic Resonance Center of the University of Colorado Health Sciences Center, where NMR experiments were carried out, received major support from the Howard Hughes Medical Institute (HHMI).

* To whom correspondence should be addressed.

10.1021/bi026608x CCC: $22.00
Published on Web 12/07/2002

because it has been shown to stabilize moderate-sized helices (*22*). The paramagnetic metal also provides additional signal dispersion in the ^{1}H NMR spectrum that has some advantage for structural characterization. Circular dichroism, two-dimensional ^{1}H NMR, and hydrogen−deuterium (H/D) exchange data are used to characterize the modified and unmodified peptides. A modification to the Lifson−Roig model is developed to extract the effect of the cross-link on the helix initiation, v^2, and propagation, w, parameters.

MATERIALS AND METHODS

General Materials. Deuterated solvents were purchased from Isotec (Miamisburg, OH). The *N*-acetyl-L-histidine-*N*-methylamide was received from Bachem (Torrance, CA). Ruthenium trichloride was purchased from Strem (Newburyport, MA). *cis*-Dichlorotetraammineruthenium(III) and sodium (ethylenediaminetetraacetato)cobaltate(III), Co(EDTA), were synthesized by literature procedures (*27*, *28*). 2,3-Dihydroxynaphthalene and hydrazine were purchased from Aldrich (Milwaukee, WI). All chemicals were used as received.

General Methods. Peptide purification was performed on a Pharmacia 2248 dual pump HPLC system, with a 2141 VWM variable-wavelength detection monitor, using either analytical or semipreparatory C18 reversed-phase columns (Vydac, model numbers 218TP1022 and 218TP104). Gradient programs were run with flow rates of 1 mL/min (analytical) or 10 mL/min (semiprep). MALDI-TOF mass spectroscopy was performed at the University of Colorado Health Sciences Center in the laboratory of Dr. John Stewart. Bradykinin was used to calibrate the mass spectrometer. UV−vis absorbance spectroscopy was performed on a Beckman DU640 absorbance spectrophotometer. Circular dichroism (CD) was performed on a Jasco J500-C spectropolarimeter. One-dimensional (1D) and two-dimensional (2D) ^{1}H NMR were performed on either a Varian Mercury 400 MHz spectrometer at the University of Denver or on Varian Inova 500 or 600 MHz NMR spectrometers at the Biomolecular Structure and Magnetic Resonance Center of the University of Colorado Health Sciences Center.

Synthesis of cis-(Bis(N-acetyl-L-histidine-N-methylamide))-tetraammineruthenium(III), a_4Ru(His)$_2$. cis-Dichlorotetraammineruthenium(III) (18.7 mg, 6.79×10^{-5} mol) was dissolved in 750 μL of HEPES buffer (100 mM, pH 7). The solution was purged with argon, in a sealed conical vial, to remove oxygen. The solution was then transferred via cannula to a sealed round-bottom flask containing freshly made zinc/mercury amalgam. The solution and amalgam were stirred under argon for 1 h.

N-Acetyl-L-histidine-*N*-methylamide (NAHMA; 85.6 mg, 4.1×10^{-4} mol) was dissolved in 100 μL of HEPES buffer in a conical vial, which was sealed and purged with argon. The reduced ruthenium solution was transferred via cannula to the vial containing the NAHMA. The solution was stirred under argon for 4−5 h. Then, Co(EDTA) (50 mg, 1.5×10^{-4} mol) was added to oxidize the ruthenium back to Ru(III), and the solution was stirred overnight.

Crude purification was done on a CM-Sepharose column using an ammonium chloride step gradient. The Co(EDTA) eluted as a purple band with 0.01 M NH_4Cl, a light yellow band was eluted with 0.05 M NH_4Cl, the desired product came off with 0.1 M NH_4Cl as an orange-pink band, and a brown band eluted with 1 M NH_4Cl. Further purification was done by HPLC using a semipreparative C18 reversed-phase column. The mobile phase was a water/acetonitrile gradient starting at 5% acetonitrile for 5 min and then from 5% acetonitrile to 30% acetonitrile at 45 min. The gradient was then brought back down to 5% acetonitrile at 50 min, and the run was finished with 5% acetonitrile (55 min). The desired product peak eluted at 15.6 min. Yield, 10 mg (25%). ^{1}H NMR (400 MHz, 20% D_2O in H_2O, 25 °C): 12.65 ppm (bs, 2H, His βH), 11.40 (bs, 2H, His βH), 8.36 (s, 2H, acetyl amide), 7.86 (s, 2H, methylamide), 4.67 (s, 2H, αH), 3.71 (bs, 2H His δH), 2.61 (s, 6H, acetyl methyl), 1.73 (s, 6H, amide methyl), ∼ −28.5 (bs, 2H, His ϵH). Assignment of His δ and ϵ protons is based on assignments for *cis*-(bis(imidazole))tetraammineruthenium(III) (*29*). Assignment of amide NH, His βH and acetyl and amide methyl groups is based on TOCSY data.

Synthesis of Ac-AHAAAHA-CONH$_2$, HisPep. The peptide was synthesized by solid phase peptide synthesis, using a BOC/benzyl protection scheme, as described previously (*30*). The peptide was cleaved from the resin with HF. The crude peptide was purified by HPLC, using a semipreparative C18 reversed-phase column. The mobile phase was a water/acetonitrile gradient starting at 5% acetonitrile for 5 min and then from 5% acetonitrile to 30% acetonitrile at 45 min. The gradient was then brought back down to 5% acetonitrile at 50 min, and the run was finished with 5% acetonitrile (55 min). ^{1}H NMR (400 MHz, 10% D_2O in H_2O, 25 °C): 8.69 (s, 2H, His ϵH), 8.49 (d, ^3J = 7.2 Hz, 1H, His NH), 8.39 (bm, 3H, His/Ala NH), 8.33 (bm, 2H, Ala NH), 8.22 (d, ^3J = 5.6 Hz, 1H, Ala NH), 7.72 (s, 1H, $CONH_2$), 7.39 (s, 2H, His δH), 7.14 (s, 1H, $CONH_2$), 4.34 (bm, 5H, Ala αH), 3.37 (dd, 2H, His βH), 3.25 (m, 2H, His βH), 2.11 (s, 3H, acetyl), 1.46 (m, 15H, Ala Me). Note: Assignments to amino acid type where indicated are based on 2D TOCSY spectra. The α-protons for the histidines are likely hidden under the water peak. In D_2O, a weak multiplet at ∼4.75 ppm is observed near the residual HOD peak, possibly due to His αH.

Ruthenium Modification of Ac-AHAAAHA-NH$_2$. cis-Dichlorotetraammineruthenium(III) (3.5 mg, 1.3×10^{-5} mol) was dissolved in 750 μL HEPES buffer. The solution was purged with argon in a sealed conical vial. The solution was transferred to a round-bottom flask containing freshly made Zn/Hg amalgam. It was stirred under argon for 1 h.

HisPep (18 mg, 1.2×10^{-5} mol) was dissolved in 100 μL HEPES buffer and purged with argon. The reduced ruthenium solution was transferred by cannula into the peptide vial and stirred under argon for 4−5 h. After that time, Co(EDTA) (9.5 mg, 2.6×10^{-5} mol) was added to reoxidize to Ru(III), and the solution was stirred overnight.

[1] Abbreviations: Ac, acetyl; $CONH_2$, carboxamide; v^2, Lifson−Roig helix initiation parameter; w, Lifson−Roig helix propagation parameter; σ, Zimm−Bragg helix initiation parameter; s, Zimm−Bragg helix propagation parameter; Co(EDTA), sodium (ethylenediaminetetraacetato)cobaltate(III); a_4Ru(His)$_2$, *cis*-(bis(*N*-acetyl-L-histidine-*N*-methylamide))tetraammineruthenium(III); HisPep, the heptapeptide, acetyl-AHAAAHA-carboxamide; RuHisPep, acetyl-AHAAAHA-carboxamide with the histidine side chains cross-linked with a *cis*-tetraammineruthenium(III) moiety; k_{ex}, intrinsic hydrogen−deuterium exchange rate constant in an unstructured peptide; $[\Theta]_{222}$, mean molar residue ellipticity at 222 nm.

The reaction mixture was purified with a CM-Sepharose column, as follows. The CoEDTA eluted with 0.01 M NH_4-Cl, the desired product eluted as a pink-orange band with ~6 M HCl. The eluted product was lyophilized and further purified on HPLC, using a semipreparative C18 reversed-phase column. The mobile phase was a water/acetonitrile gradient starting at 5% acetonitrile for 5 min, and then from 5% acetonitrile to 30% acetonitrile at 45 min. The gradient was then brought back down to 5% acetonitrile at 50 min, and the run was finished with 5% acetonitrile (55 min). The desired product came off at 24.5 min. Yield, 5 mg (50%). MALDI-TOF MS; calcd. (*m*/*e*) 857.77; found, 856. ^{1}H NMR characterization methods are described below.

pH Titration Experiments. The experiments were performed on a Beckman DU-640 spectrometer. Samples of $a_4Ru(His)_2$ and Ru(III) cross-linked Ac-AHAAAHA-$CONH_2$ (RuHisPep) were dissolved in 20 mM Tris, and measurements were made in 1 cm path length quartz cuvettes. Solution concentrations for $a_4Ru(His)_2$ and RuHisPep, here and in other experiments, were estimated using the published extinction coefficients (below pH ~6, $\epsilon_{286} = 1390\ M^{-1}\ cm^{-1}$, and $\epsilon_{310} = 1914\ M^{-1}\ cm^{-1}$) for *cis*-(bis(imidazole))tetraammineruthenium(III) (*29*). The pH was adjusted in steps of 0.25−0.30 from pH 4 to pH 11 by removing 2 μL of the solution and adding 1 μL of a 2X sample solution and 1 μL of an appropriate concentration of NaOH. The pH was measured with a Corning 220 pH meter. The acid equilibrium was monitored at 320 nm. The absorbance was plotted versus pH using SigmaPlot (v.4). The pK_a was extracted by fitting the data to the Henderson−Hasselbalch equation:

$$y = \{a + b^{*}10^{n(pK_a - pH)}\}/\{1 + 10^{n(pK_a - pH)}\} \qquad (1)$$

In this equation y is the absorbance at the measured wavelength, a and b are the high pH and low pH limits of absorption at that wavelength, respectively, and n is the number of protons involved in the process.

Circular Dichroism Experiments. Circular dichroism was used to determine the α-helix content of HisPep and RuHisPep under different conditions. The CD spectrometer was calibrated with (1*S*)-(+)-10-camphorsulfonic acid (*31*). CD spectra were scanned from 350 to 200 nm. The peptide concentrations ranged from 20 to 150 μM.

Titration with EDTA was carried out in 1 M NaCl, 1 mM sodium phosphate, 1 mM sodium citrate, 1 mM sodium borate, pH 7. The temperature was maintained at 1 °C with a circulating water bath (Fisher-Scientific, model 9110). Solution temperature was measured directly with a thermocouple (Digisense, Cole-Palmer). The HisPep concentration was 138 μM. One microliter volumes of 0.5 M EDTA (pH 7.05) were added to the HisPep solution. EDTA was added to the peptide solution until a concentration of 1 mM was reached. Ellipticity measurements were made at 325 nm (baseline) and 222 nm (helix) at each [EDTA].

The temperature dependence of the RuHisPep CD signal at 222 nm was monitored from 0 to 60 °C in 1 M NaCl, 1 mM sodium phosphate, 1 mM sodium citrate, 1 mM sodium borate, pH 7. Temperature was controlled and measured as described above. The temperature dependence of the mean molar residue ellipticity at 222 nm, $[\Theta]_{222}$, was fit with a modified Lifson−Roig model (see Discussion) with the enthalpy for the propagation parameter, w, set to −0.8 kcal/mol.

The $[\Theta]_{222}$ values were converted to fractional helicity using eq 2 (*32*)

$$f_H = ([\Theta]_{222} - \Theta_C)/(\Theta_H - \Theta_C) \qquad (2)$$

where Θ_H is the baseline ellipticity for a complete helix and Θ_C is the baseline ellipticity for a random coil. The values for Θ_H and Θ_C as a function of temperature, T, are (*32*, *33*)

$$\Theta_H = (-44\,000 + 250T)(1 - x/N_r) \qquad (3)$$

$$\Theta_C = 2220 - 53T \qquad (4)$$

where N_r is the number of amino acid residues in the peptide. The value of −44 000 is the per residue ellipticity for an infinite helix and 2220 is the per residue value for a random coil, both at 0 °C in H_2O at 222 nm, and $x = 3$ accounts for helix end effects and is the number of non-hydrogen bonded carbonyl units at the C-terminus (*32*, *33*).

NMR-Monitored Kinetic H/D Exchange Experiments. The intrinsic exchange rates, k_{ex}, of the left (acetyl-NH) and right (methylamide) amide NH's of the model compound, $a_4Ru(His)_2$, were determined to permit evaluation of the intrinsic exchange rates in the ruthenium-modified peptide. The rates were measured on the amide protons of $a_4Ru(His)_2$ at 8.36 (left) and 7.86 (right) ppm. The complex was dissolved in ice-cold 50 mM acetic acid-d4 in D_2O and immediately transferred to an ice-cold NMR tube. The sample was inserted into the probe of the NMR spectrometer (400 MHz) which was equilibrated to 1 °C. The first 1D spectrum was acquired within 5 min of dissolving the $a_4Ru(His)_2$. The rates were measured over a pH* range from 1.5 to 4.5. The rates at each pH* were obtained by plotting fractional proton occupancy versus time and fitting the data to a single-exponential curve. The rate constants, k_{ex}, were then plotted versus corrected pH (pH* + 0.4, *34*) and fit to eq 5 (*35*):

$$k_{ex} = k_A 10^{-pD} + k_B 10^{[pD - pK_D]} + k_W \qquad (5)$$

where k_A is the second-order rate constant for acid catalysis, k_B is the second-order rate constant for base catalysis, and k_W is the second-order rate constant for water catalysis of exchange, pK_D is the D_2O dissociation constant (15.83, at 1 °C) and pD is corrected pH. Curve fitting was performed with Kaleidagraph software.

The correction factors for acid (A) and base (B) exchange rates for the right (R) and left (L) amides (A_L, A_R, B_L, B_R) were calculated versus an alanine dipeptide (ref *35*; corrected from 5 °C to 1 °C using E_a(base) = 2.6 kcal/mol, E_a(acid) = 15 kcal/mol, and E_a(water) = 13 kcal/mol, see ref *36* and http://www.fccc.edu/research/labs/roder/sphere/) using eq 6 (*35*):

$$\log A(B)_{L/R} = \log k_{ex}\,(a_4Ru(His)_2) - \log k_{ex}\,(Ala) \qquad (6)$$

where $\log k_{ex}$ ($a_4Ru(His)_2$) and $\log k_{ex}$ (Ala) are the logarithms of the acid or base-catalyzed exchange rate constants of the right or left amide NH, as appropriate, for $a_4Ru(His)_2$ and Ala.

For H/D exchange studies on HisPep and RuHisPep the methodology was the same as for $a_4Ru(His)_2$, except that the RuHisPep NMR data were obtained at 500 MHz. The same D_2O buffer was used with pH* in the range 3.3−3.7.

For HisPep, exchange experiments were also carried out with either 5 or 10 mM EDTA-d16 added to the 50 mM acetic acid-d4 buffer. The integrated intensity from 1D NMR spectra for the entire amide region (HisPep) or of individual amides (RuHisPep) was followed as a function of time. For HisPep these data were converted to fractional proton occupancy, as previously described (*30*). The intrinsic rate constants for exchange, k_{ex}, for the amide NH's of HisPep at a given pH* were calculated using the web-based program, Sphere (see refs *35* and *36* and http://www.fccc.edu/research/labs/roder/sphere/). An MS Excel implementation of Sphere was used to calculate k_{ex} for amide NH's which have the Ru(III)-modified histidine on one side, using the acid and base exchange correction factors (A_L, A_R, B_L, B_R) for a_4Ru-$(His)_2$ determined as described above. The oligopeptide reference state was used in calculations since these are small peptides and the exchange behavior of small peptides is modeled well with this reference state (*35*).

The intrinsic rate constants for exchange of the amide NH's of the unmodified Ac-AHAAAHA-$CONH_2$ peptide were used to calculate the bulk exchange rate for this peptide using the methods of Baldwin and co-workers (*14*), as described previously (*30*). The fractional hydrogen bonding for the amide NH of each residue *i*, $f_{HB}(i)$, was obtained from the fractional helicity of the $i - 2$ residue, $f_H(i-2)$, using the Lifson−Roig helix−coil theory (in the Lifson−Roig theory, helicity at residue $i - 2$ indicates a hydrogen bond between the $i - 4$ carbonyl and the *i* amide NH) as implemented by the program, Helix2 (*7*), or a locally written MathCad file (v. 7.03, MathSoft, Inc.). A modification of the Lifson−Roig helix−coil theory (see Discussion) implemented in a MathCad file was used to determine $f_H(i-2)$ and, thus, $f_{HB}(i)$ for RuHisPep.

The fractional proton occupancy as a function of time, $f_o(t)$, can be expressed as in eq 7 (*14*):

$$f_o(t) = \sum(1/N_r)\exp[-(k_{ex}[1 - f_{HB}(i)])t] \qquad (7)$$

where N_r is the number of residues in the peptide ($N_r = 7$ for HisPep). For RuHisPep, $f_o(t)$ is calculated for individual amide NH's ($N_r = 1$ and the summation is dropped from eq 7). For the N-terminal amide of these peptides (Ac−NH−Ala), the k_{ex} data for the left side amide of *N*-acetylalanine methylamide (*35*) was used to calculate k_{ex} at a given pH*.

NMR Experiments on RuHisPep. To extract structural information for RuHisPep, TOCSY and ROESY 2D NMR experiments were performed at 600 MHz. The TOCSY was used to establish amino acid spin systems, and the ROESY was used to provide sequential assignment of the peptide and to determine medium range structural interactions.

For the TOCSY, the sweep width was set to 16 000 Hz, t_1 was set to 256 increments with 80 scans per increment and 4096 points per scan. The mixing time was set to 19.7 ms. For the ROESY, the sweep width was set to 8000 Hz, t_1 was set to 256 increments with 88 scans per increment and 4096 points per scan. The spin lock field was set to 4.3 kHz, and the mixing time was 75 ms. The pulse width and water saturation frequency were optimized before both experiments. Both experiments were operated at 17.5 °C, which is a compromise between peak sharpness (at higher temperatures) and peak overlap. Sample concentration was ~2 mM, and the buffer was 50 mM acetic acid-d4 in 10% D_2O, pH 3.5. The data were analyzed with NMRpipe software, using a shifted sine squared weighting function.

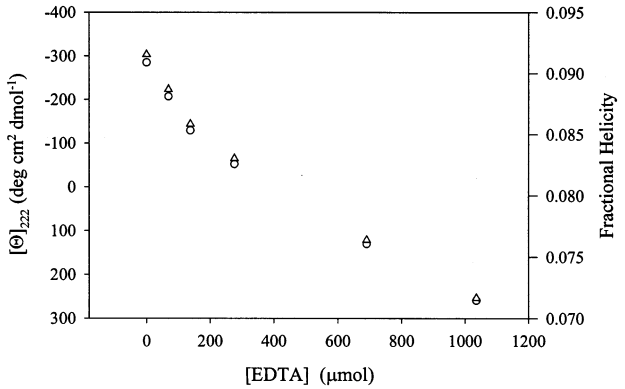

FIGURE 1: EDTA titration, monitored at 222 nm by circular dichroism, of Ac-AHAAAHA-$CONH_2$ at a concentration of 138 μM. The temperature was 0 °C. The buffer was 1 M NaCl, 1 mM sodium phosphate, 1 mM sodium citrate, 1 mM sodium borate, pH 7. The open circles are the mean molar residue ellipticity at 222 nm, $[\Theta]_{222}$, and the open triangles are the fractional helicity evaluated using $[\Theta]_{222}$ as described in the Materials and Methods.

Three-bond $C_\alpha H-NH$ coupling constants, $^3J(C_\alpha H-NH)$, as a function of temperature were obtained from 1D NMR spectra collected at 500 MHz. A sweep width of 14 000 Hz was used, and 28 000 points were collected per scan. The spectra were zero-filled to a digital resolution of 0.21 Hz/point. The FID was treated with a Gaussian apodization function (Gaussian time constant of 0.686) prior to Fourier transformation.

RESULTS

Characterization of the Heptapeptide Ac-AHAAAHA-$CONH_2$. Short peptides are expected to be essentially devoid of any persistent structure. For Ac-AHAAAHA-$CONH_2$ (HisPep), the poor helical propensity of the histidine side chain (*7*) should accentuate the lack of a tendency to populate helical conformations. This expectation is largely confirmed by standard spectroscopic methods. The NMR spectrum shows poor chemical shift dispersion with the chemical shifts (see Material and Methods) clustering around the random coil values for alanine (for GGAGG: NH, 8.35 ppm; $C_\alpha H$, 4.33 ppm, $C_\beta H$ = 1.45 ppm) and histidine (for GGHGG: NH, 8.52 ppm; $C_\alpha H$, 4.75 ppm; $C_\beta H$, 3.20, 3.35 ppm; $C_\delta H$, 7.32 ppm; $C_\epsilon H$, 8.59 ppm) residues (*37*). Perhaps not surprisingly, this short peptide binds metal contaminants, presumably available in buffer salts. The mean molar residue ellipticity at 222 nm, $[\Theta]_{222}$, indicated a fractional helicity of approximately 0.09 in buffer at 0 °C. As EDTA is added to the solution, the $[\Theta]_{222}$ becomes progressively more positive with a fractional helicity approaching 0.07 for [EDTA] = 1 mM (see Figure 1). The helix parameters of Baldwin and co-workers predict a fractional helicity of 0.02 for this peptide (*7*). The structural properties of this peptide were also studied by NMR H/D exchange methods. A similar sensitivity of the experiment to the presence of the metal chelating ligand EDTA was also observed. A significant slowing of the amide H/D exchange relative to prediction was observed in the absence of EDTA (see Figure 2). The presence of either 5 or 10 mM EDTA (Figure 2) gave amide H/D exchange data that agreed reasonably well with Lifson−Roig helix coil theory, using the helix propagation parameters

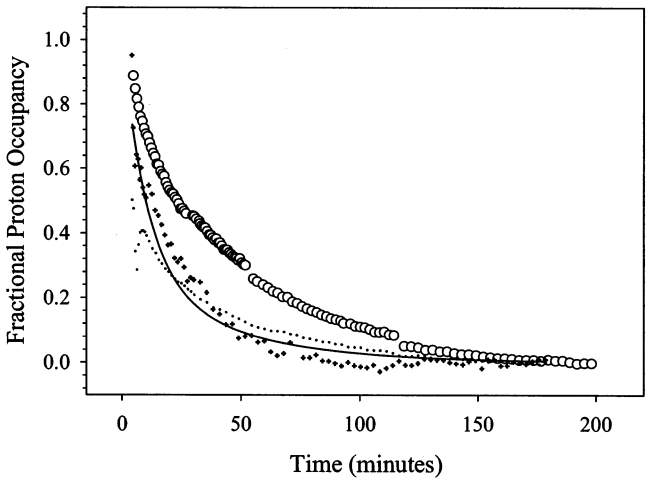

FIGURE 2: Kinetic proton exchange of the histidine peptide with and without EDTA. The temperature was 1 °C. The buffer was 50 mM acetic acid-d_4 in D_2O. The open circles represent exchange without EDTA. The dots represent exchange with 5 mM EDTA-d16. The crosses represent exchange with 10 mM EDTA-d16. The pH* of the 0 and 10 mM EDTA solutions was 3.34, and the pH* of the 5 mM EDTA solution was 3.48. The solid line represents the Lifson−Roig fit (eq 7) to the 10 mM EDTA-d16 data (pH* 3.34; the effect of fitting the data at pH* 3.48 is small).

of Baldwin and co-workers (*7*). There is some deviation from the predicted H/D exchange decay curve; however, deviations of this magnitude are not uncommon in this type of data (*14*, *32*) and probably stem from the ∼5 min dead time of H/D exchange NMR experiments and approximation of 100% proton occupancy by linear extrapolation back to time zero (*14*, *30*). For HisPep, the problem is magnified by the greater uncertainty in the parameters defining the intrinsic H/D exchange rates for histidine (*35*).

Ruthenium Tetraammine Cross-Linked Ac-AHAAAHA-CONH₂. The heptapeptide, Ac-AHAAAHA-$CONH_2$, was reacted with *cis*-dichlorotetraammineruthenium(II) followed by oxidation with CoEDTA to give the substitution inert Ru(III) oxidation state. The resulting cross-linked peptide, RuHisPep, was then purified by ion exchange and reversed-phase chromatography (see Materials and Methods). MALDI-TOF mass spectral data gave a molecular ion with *m*/*e* of 856 in good agreement with the expected value of 857.77 *m*/*e*. The CD spectrum is now characteristic of an α-helix (see Figure 3a), with a negative peak near 222 nm. The temperature dependence of $[\Theta]_{222}$ is shown in Figure 3b. Initially $[\Theta]_{222}$ drops; however, above 40 °C $[\Theta]_{222}$ appears to levels off. However, due to the convergent temperature dependence of the Θ_H and Θ_C baselines in eqs 3 and 4, the fractional helicity derived from eq 2 continues to decrease slowly with temperature.

UV−Vis Titrations of RuHisPep. To aid in interpretation of the data, a simple model for the ruthenated histidine cross-link, the metal complex *cis*-(bis(*N*-acetyl-L-histidine-*N*-methylamide))tetraammineruthenium(III), $a_4Ru(His)_2$, was also prepared. Binding of the ruthenium moiety to the imidazole ring of histidine is expected to dramatically shift the pK_a of the NH of the imidazole ring and this can be readily monitored spectroscopically (*22*, *29*). Figure 4a shows a pH titration of the UV−vis spectrum for the $a_4Ru(His)_2$. It is clear that part way through the titration (above ∼pH 9), the initial isosbestic point at 330 nm in lost. A plot of the

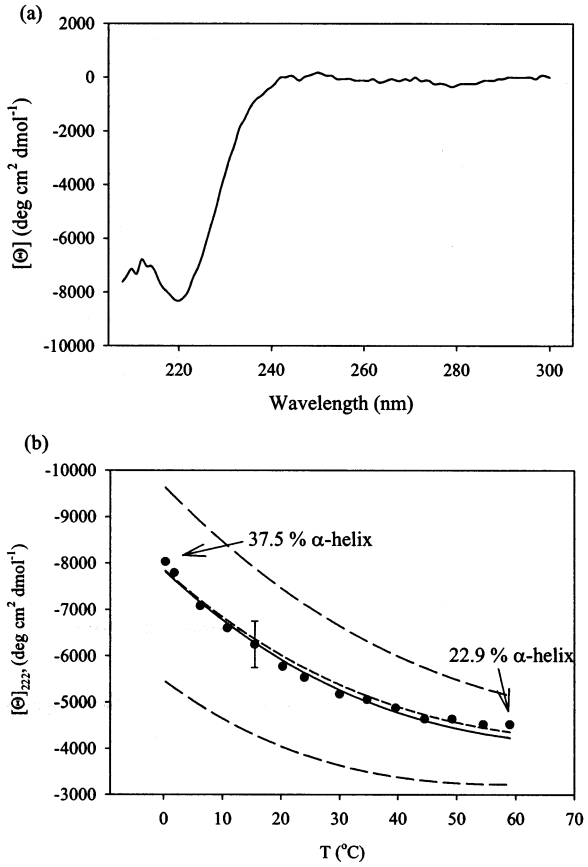

FIGURE 3: (a) Circular dichroism spectrum of RuHisPep at 0.3 °C. Mean molar residue ellipticity, [Θ], is plotted vs wavelength in nm. (b) Temperature dependence (solid circles) of mean molar residue ellipticity at 222 nm, $[\Theta]_{222}$, of RuHisPep. The solid line is a fit of the data to the modified Lifson−Roig helix−coil theory described in the Discussion. The enthalpy used for the propagation parameters, *w*, of all residues was −0.8 kcal/mol. The best fit is obtained with $(\upsilon_{35})^2 = 0.0088$. The long dashed lines above and below the data show the predicted curves obtained when $(\upsilon_{35})^2$ is increased (above, $(\upsilon_{35})^2 = 0.011$) or decreased (below, $(\upsilon_{35})^2 = 0.0066$) by 25%. The short dashed line is a fit of the data with $(\upsilon_{35})^2 = 0.0187$ and $w = 1.07$ for alanine to account for context-dependent Lys stabilization according to ref 48. The buffer is 1 M NaCl, 1 mM sodium phosphate, 1 mM sodium citrate, 1 mM sodium borate, pH 7. The concentration of RuHisPep is 24 μM.

data at 320 nm (Figure 4a, inset) yields two pK_a values, 8.1 and 10.4 (pK_a for the NH of free imidazole is ∼14.5, ref *38*). These are similar to the values of 9.1 and 10.5 reported for a *cis*-(bis(imidazole))tetraammineruthenium(III) complex (*29*). Titrations were carried out for RuHisPep (Figure 4b) and yielded two pK_a values, 7.9 and 10.1 (Figure 4b, inset), similar to the values for $a_4Ru(His)_2$. The lower pK_a value for RuHisPep is similar to the pK_a of 7.5 reported previously for a 17 residue alanine-based peptide with an *i*,*i*+4 histidine cross-link at the C-terminal end (ref *22*, the higher pK_a for the other histidine NH was not reported for this peptide). Thus, the UV−vis pH titration data for RuHisPep is characteristic of a *cis*-tetraammineruthenium(III) moiety cross-linking two histidines.

Two-Dimensional NMR Studies of RuHisPep. The additional signal dispersion provided by the paramagnetic Ru(III) cross-link permits unambiguous assignment of all residues in the NMR spectrum of RuHisPep without the necessity for costly site-selective deuteration (*25*) or ^{15}N-labeling (*15*). This advantage is somewhat counterbalanced

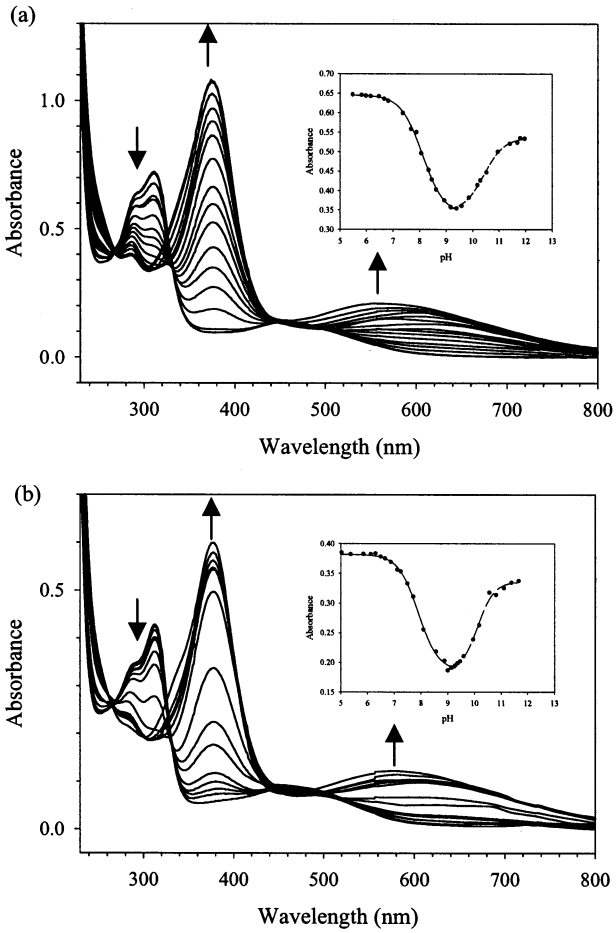

FIGURE 4: (a) pH titration of $a_4Ru(His)_2$ at 43 μM concentration in 20 mM Tris solution. Spectra from top to bottom (at 280 nm) are at pH 6.67, 6.82, 7.37, 7.68, 7.88, 8.06, 8.34, 8.46, 8.62, 8.93, 9.16, 9.39, 9.58, 9.86, 10.18, and 10.29. The inset shows the pH dependence of absorbance at 320 nm. The solid line is a fit of the low pH titration to the Henderson−Hasselbalch equation, and the dashed line is a fit of the high pH titration to the Henderson−Hasselbalch equation. The pK_a values are reported in the text. (b) pH titration of RuHisPep at 23 μM concentration in 20 mM Tris solution. Spectra from top to bottom (at 280 nm) are at pH 6.49, 6.66, 6.87, 7.11, 7.24, 7.49, 7.71, 8.09, 8.83, 9.14, 9.27, 9.36, 9.59, and 9.95. The inset shows the pH dependence of absorbance at 320 nm. The solid line is a fit of the low pH titration to the Henderson−Hasselbalch equation, and the dashed line is a fit of the high pH titration to the Henderson−Hasselbalch equation. The pK_a values are reported in the text. The arrows, in both panels, indicate the direction in which absorbance changes for the absorbance band below the arrow as pH is increased.

by the broadening of a number of ^{1}H resonances which creates difficulties for 2D experiments with significant mixing times. Figure 5 presents a section of the ROESY spectrum of RuHisPep showing sequential $d_{\alpha N}$ and $d_{\beta N}$ connectivities that allow resonance assignment (*39*). The ^{1}H resonance assignments derived from ROESY and TOCSY spectra are summarized in Table 1. Figure 5 also shows a cross-peak from an imidazole ring proton to the amide NH of Ala 7. This observation permits assignment of the His 6 and His 2 ring protons. On the basis of model studies (HyperChem, release 3), the presence of this cross-peak can only be reconciled with binding of the ruthenium to the δ-nitrogen of the imidazole ring of His 6. Using a simple MM+ force field minimization (of the tetraammineruthenium-(III) cross-linked histidine side chain unit alone with

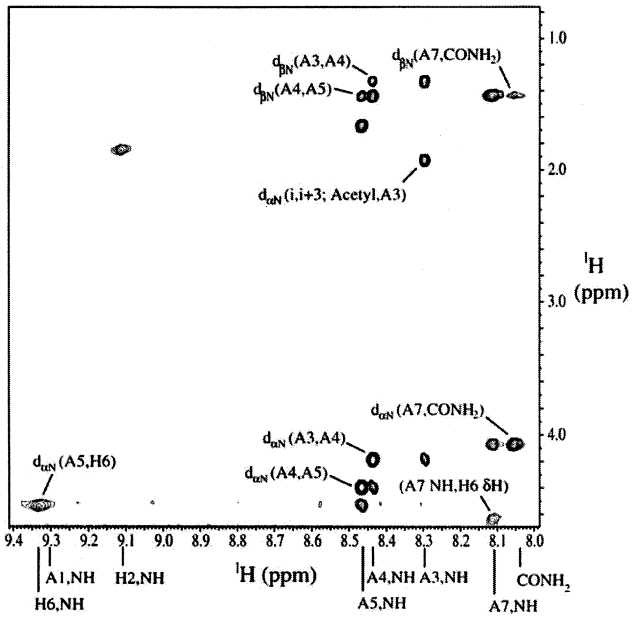

FIGURE 5: ROESY spectrum of RuHisPep in the amide NH/C_αH,C_βH region. Sequential and medium range $d_{\alpha N}$ cross-peaks are labeled. The chemical shifts of the amide NH protons are indicated below the t_2 axis. Data were collected at 17.5 °C in 50 mM acetic acid-d4, pH 3.5, 10% D_2O. A sequential $d_{\alpha N}$ cross-peak between Ala 1 C_αH and His 2 NH, not seen in this figure, is observed at 9.11/5.25 ppm.

Table 1: ^{1}H NMR Assignments of RuHisPep at 600 MHz and 17.5 °C[a]

residue	NH	α	β	others
Ala 1	9.31	5.25	1.00	acetyl 1.93
His 2	9.11	7.32[b]	1.85	δCH −0.21, ϵCH 6.59,[c] δNH −0.02[b]
Ala 3	8.30	4.19	1.33	
Ala 4	8.44	4.39	1.44	
Ala 5	8.47	4.54	1.67	
His 6	9.33	5.65[b]	8.73,[b] 16.19[b]	δCH 4.64, ϵCH 11.94,[b] ϵNH 2.93[b,d]
Ala 7	8.11	4.07	1.43	$CONH_2$ 8.05[e]

[a] Chemical shifts referenced to DSS are taken from the position of cross-peaks in the 2D ROESY and TOCSY spectra, unless otherwise noted. [b] Strongly broadened resonances. Line widths were measured in the 1D 600 MHz spectrum Fourier transformed using a sine bell constant of 0.128 and a sine bell shift of −0.128. The line width at half-height for the indicated resonances is as follows: His 2 αH, 84 Hz; His 2 δNH, ∼90 Hz; His 6 αH, 39 Hz; His 6 βH (16.19 ppm), 97 Hz; His 6 βH (8.73 ppm), 59 Hz; His 6 ϵCH, 73 Hz; His 6 ϵNH, 137 Hz. The line widths of other resonances are in the range 7.6 (acetyl methyl) to 25 Hz (His 2 δCH). [c] Assignment of ϵCH versus δCH for His 2 is based on slow H/D exchange of the resonance at 6.59 ppm in H/D exchange experiments on RuHisPep. [d] Resonance position taken from the 1D spectrum. [e] In the 1D spectrum at 17.5 °C, the two $CONH_2$ ^{1}H resonances are partially resolved, giving chemical shifts of 8.05 and 8.04 (upfield shoulder) ppm.

Ac-AHAAAHA-$CONH_2$ held in an α-helical conformation or minimization of the whole peptide after minimization of the cross-link), the ruthenium binding to δN of His 6 and ϵN of His 2 gives a His 6 δH to Ala 7 NH distance of 2.4 ± 0.2 Å. When His 6 is bound to ruthenium via the ϵN the His 6 δH and ϵH to Ala 7 NH distances are >5 Å. The unusual chemical shifts of the β-protons of His 6 (Table 1) are also consistent with His 6 δN ruthenium binding. The model studies indicate that these protons are 3.2−3.5 Å from the ruthenium with His 6 δN ruthenium binding. With His 2 bound through the ϵN to ruthenium, the model studies indicate that both His 2 β-protons are >5.5 Å from the

Table 2: Temperature Dependence of $^3J(C_\alpha H-NH)$ at 500 MHz

	$^3J(C_\alpha H-NH)$ (Hz)[a]		
temperature (°C)	Ala 3	Ala 4[b]	Ala 5[b,c]
5	3.9	4.4	–
10	4.3	4.8	3.0
15	4.4	5.0	3.2
20	4.5	5.3	4.0
25	4.7	–	–
30	4.2	–	–
35	4.7	–	–

[a] Estimated error ±0.2 Hz [b] Above 20 °C, the NH resonances of Ala 4 and Ala 5 overlap precluding measurement of the $^3J(C_\alpha H-NH)$ coupling constants. [c] The $^3J(C_\alpha H-NH)$ coupling constant for Ala 5 is not resolved at 5 °C.

ruthenium, consistent with the more normal chemical shift for the His 2 β-protons. For His 2 bound to ruthenium through the δN, one His 2 β-proton is always ~3.2 Å from the ruthenium and the other ~4.5 Å. Their chemical shifts would be expected to be substantially different and they are in fact coincident. Thus, models studies indicate that the His 6 δN/His2 ϵN binding mode for ruthenium is the only one consistent with the NMR data.

The NMR data also provide some information on the conformational constraints on RuHisPep. One medium range cross-peak is observed in the ROESY spectrum, a strong $d_{\alpha N}(i,i+3)$ connectivity between the acetyl methyl and the amide NH of Ala 3 (see Figure 5), as expected for an α-helix (*39*). The inability to observe a $d_{\alpha N}(i,i+3)$ connectivity for His2/Ala 5 may be limited by broadening of the His 2 $C_\alpha H$ resonance (see Table 1). Connectivities between adjacent amide NH's are usually observed in α-helical structure (*39*). A weak d_{NN} connectivity between Ala 5 and His 6 is observed. Lack of sufficient chemical shift separation (A4/A5 and A3/A4) may affect the ability to observe other d_{NN} connectivities. No $d_{\alpha\beta}(i,i+3)$ connectivities are observed as would be expected for an α-helix (*39*). For His2/Ala5 and Ala3/His6, broadening of the His 2 $C_\alpha H$ and the His 6 β-protons (see Table 1) likely limit the ability to observe these couplings. For Ala4/Ala7, unfortunately the methyl resonances are coincident. In sum, two connectivities consistent with a helical conformation are observed, but resonance overlap and line broadening caused by the paramagnetic ruthenium limit the ability to observe other connectivities expected for helical structure.

Scalar couplings between the amide NH and $C_\alpha H$ of a residue, $^3J(C_\alpha H-NH)$, also provide structural information. Typically, *J*-couplings <5 Hz are characteristic of helical structure (*39*, *40*). The amide NH resonances of alanines 3, 4, and 5 are sufficiently sharp to allow determination of the $^3J(NH-C_\alpha H)$ coupling from 5 to 35 °C. The $^3J(C_\alpha H-NH)$ coupling constants are in the range 3.0−4.8 Hz at 5 and 10 °C (Table 2) and increase slowly as temperature is raised, consistent with the loss of helical structure observed by CD as a function of temperature (Figure 3b). The low values for $^3J(C_\alpha H-NH)$ indicate significant population of the α-region of ϕ,ψ space, even at higher temperatures. Taken together, the $^3J(C_\alpha H-NH)$ data and the available d_{NN} and $d_{\alpha N}(i,i+3)$ data are consistent with substantial population of the α-region of ϕ,ψ space for RuHisPep.

Hydrogen Exchange Studies. We also studied the hydrogen exchange properties of RuHisPep. In conjunction with these

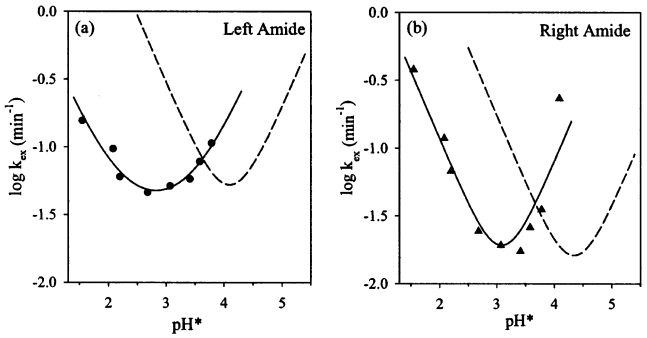

FIGURE 6: Log k_{ex} vs pH* plots for the (a) left side (AcNH-) and (b) right side (−$NHCH_3$) amides of $a_4Ru(His)_2$. Data were acquired at 1 °C in 50 mM acetic acid-d4. The solid curves are fits of the data to eq 5, Material and Methods. For the left side amide, the fit to eq 5 gives log $k_A = 1.10$, log $k_B = 10.48$, and log $k_W = -1.49$. For the right side amide, the fit to eq 5 gives log $k_A = 1.47$ and log $k_B = 10.33$ (k_W set to 0). The dashed lines are data for the corresponding amides of *N*-acetyl-L-alanine-*N*-methylamide taken from ref *35*. The k_B, k_A, and k_W rates constants for *N*-acetyl-L-alanine-*N*-methylamide were adjusted to 1 °C from the reported values at 5 °C for comparison with the $a_4Ru(His)_2$ data, using E_a(acid) = 15 kcal/mol, E_a(base) = 2.6 kcal/mol, and E_a(water) = 13 kcal/mol (*36*).

experiments, we measured the intrinsic hydrogen exchange rate constants for the $a_4Ru(His)_2$ model complex. These data provide the intrinsic amide exchange rates for the cross-linked amino acid unit in the absence of surrounding peptide structure and are necessary to calibrate exchange protection for this unit due to structure induced when the unit is incorporated into a peptide. Plots of log k_{ex} versus uncorrected pH (pH*) are shown in Figure 6. As for histidine (*35*), the region around the log k_{ex} minimum is broader for the left amide NH and sharper for the right amide NH, indicating a larger contribution from k_w for the left amide NH exchange, near the minimum pH for k_{ex}, pH^*_{min}. In fact the best fit of the right amide NH data to eq 5 gave a negative value for k_w, so k_w was set to 0 for the fit shown in Figure 6b. In comparison to histidine, both the left and right amides show a small decrease in pH^*_{min} of ~0.3 units. The strong polarizing effect of the nearby Ru^{3+} may be responsible for this shift. The rate of exchange at pH^*_{min} is also slower for $a_4Ru(His)_2$ than for histidine. The effect is small for the right amide NH, but is almost a full log unit for the left side amide NH. This is presumably a steric effect caused by the proximity of the two cross-linked histidines. As with the steric effect observed for aliphatic and aromatic sides chains, the effect is most pronounced for the left side amide NH because of its proximity to the side chain. The acid correction factors (eq 6) versus alanine are log $A_L = -1.60$ and log $A_R = -1.17$. The base correction factors (eq 6) versus alanine are log $B_L = 0.80$ and log $B_R = 1.35$.

Since the amide NH NMR resonances of RuHisPep are resolved, it is possible to determine the exchange rates, k_{obs}, for each individual residue and to compare these to k_{ex} values calculated with the appropriate residue specific correction factors. Typical proton decay curves for RuHisPep are shown in Figure 7. In Table 3, the k_{obs} for H/D exchange, the observed protection factors (P_{obs}), and predicted protection factors (P_{pred}) are presented. Surprisingly, P_{obs} is largest at the ends of the helix and least in the middle of the helix. Within the center of the helix, qualitatively the protection factors for Ala 4, Ala 5, and His 6 increase progressively,

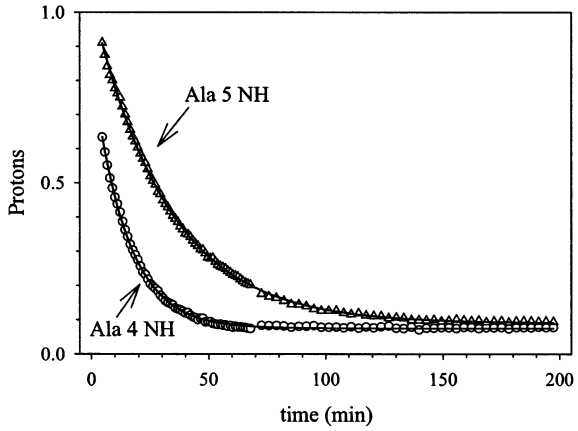

FIGURE 7: Proton decay curves for select amide NH protons of RuHisPep. Data for Ala 5 NH (open triangles) and Ala 4 NH (open circles) were acquired at 1 °C and pH* = 3.61 in 50 mM acetic acid-d4. Solid curves are fits of the data to a single-exponential decay function.

Table 3: Hydrogen−Deuterium Exchange Data for Amide NH Protons of RuHisPep at pH* 3.61 and 1 °C

amide NH	k_{ex}, (min^{-1})[a]	k_{obs} (min^{-1})[b]	observed protection factor, P_{obs}[c]	predicted protection factor, P_{pred}[d]
Ala1[e]	0.059[f]	0.069 ± 0.002[e]	0.86 ± 0.03	1
His2	0.168	0.027 ± 0.001	6.2 ± 0.3	1
Ala3	0.576	0.040 ± 0.001	14.4 ± 0.4	1
Ala4	0.034	0.071 ± 0.001	0.48 ± 0.01	1.48
Ala5	0.034	0.032 ± 0.001	1.06 ± 0.03	1.90
His6[e]	0.168	0.069 ± 0.002[e]	2.4 ± 0.1	2.02
Ala7	0.576	0.118 ± 0.001	4.9 ± 0.1	1.68

[a] k_{ex} is calculated as described in Materials and Methods. [b] k_{obs} is obtained from a single-exponential fit of the proton occupancy as a function of time for each amide NH. [c] Observed protection factor, $P_{obs} = k_{ex}/k_{obs}$. [d] The fractional hydrogen bonding, $f_{HB}(i)$, at each amide is given by the fractional helicity of the residue two residues N-terminal to the amide NH, $f_H(i-2)$. The $f_H(i-2)$ values are obtained from the partition function of the modified Lifson−Roig model described in the Discussion. $P_{pred} = 1/(1 - f_{HB}(i))$. [e] The Ala 1 and His 6 amide NH resonances are not resolved adequately in the 1 D spectrum to determine individual rate constants. [f] The Ala1 NH exchange rate is determined using the exchange rate constants for the left amide (Ac−NH) of *N*-acetyl-L-alanine methylamide reported in ref *35*, as described in Materials and Methods.

as expected (compare P_{obs} and P_{pred}, Table 3). We note that His 6 overlaps with Ala 1 so the protection factor for His 6 is somewhat uncertain. The P_{obs} for Ala 7, however, continues to increase rather than showing the expected decrease. Similarly, Ala 3 and His 2 NH's, which should not be protected, show significant protection. The Ala 1 NH shows no protection.

DISCUSSION

Structural Properties of RuHisPep. In the absence of a Ru(III) cross-link, the CD and NMR spectra of Ac-AHAAAHA-$CONH_2$, HisPep, indicate that very little ordered structure is present (Figure 1). The $[\Theta]_{222}$ is very small, and the chemical shifts are similar to random coil values. The NMR H/D exchange data are also consistent with the predictions of the Lifson−Roig theory for such a short peptide (Figure 2). Essentially no exchange protection is afforded by structure formation. Not surprisingly (*21*), the peptide shows a tendency to bind metal contaminants present in the buffer, as shown by the sensitivity of the CD spectrum and the NMR H/D exchange data to the presence of EDTA.

Binding of the substitution inert metal, Ru(III), dramatically affects the structural properties of this short peptide. The presence of the *cis*-tetraammineruthenium(III) cross-linked histidines is clearly indicated by mass spectral data, and the characteristic pH dependence of the UV−vis spectrum (Figure 4) of this moiety (*22*, *29*). The CD spectrum (Figure 3) is now typical of the presence of α-helix and shows a curved temperature dependence, as expected for loss of organized structure (*41*). The CD data is consistent with ∼37.5% helix content at 0 °C, which is more than a 10-fold enhancement over the helix content of ∼2% expected for this peptide in the absence of the cross-link. While this increase is impressive, a hexapeptide with two side-chain lactam cross-links appears to be essentially completely helical (*19*), as is a four residue (AAAQ) peptide appended to the end of a metal binding loop derived from calmodulin, when La^{3+} is added (*26*). This comparison suggests that the Ru(III) cross-link may not be as efficient a helix nucleator as these other nucleation methods; however, the synthetic ease of helix nucleation with this metal cross-link and the substantial enhancement in helix content still make this method of nucleation of great utility.

A couple of considerations are required when using CD data to estimate helix content for this Ru(III) cross-linked peptide. First, *cis*-(bis-(imidazole)tetraammine)ruthenium(III) chloride does absorb at 220 nm ($\epsilon_{220} \sim 3000\ M^{-1}\ cm^{-1}$, see ref *29*), and thus, a contribution of this moiety to the far UV CD is possible (*42*). However, previous data suggest that the contribution of this moiety to the far UV CD spectrum of peptides is small (*22*). Similarly, we have shown via direct comparison of H/D exchange and CD data that the contribution of a ruthenium amino acid to CD-derived helix parameters is small (*30*). Second, quantitative assessment of helix content in short peptides is made difficult by end effects (*26*, *43*, *44*). Gans et al. (*44*) report that x in eq 3 may be as high as 3.6. (For a peptide with an N-terminal acetyl group and a C-terminal carboxamide, x equals 4.6 when counting peptide units, as in ref *44*. But x equals 3.6 when counting residues, as in eq 3.) Using $x = 3.6$ in eq 3, we obtain a helix content of 43.5% for the lowest temperature point (0.3 °C) in Figure 3b, instead of 37.5%. In the past, Baldwin and co-workers have used $x = 2.5$ to evaluate the end effect in eq 3 (*45*). With $x = 2.5$ in eq 3, we obtain a helix content of 33.6% for the lowest temperature point in Figure 3b. These comparisons provide an estimate of the magnitude of the error involved in quantitative assessment of helix content with CD for RuHisPep.

Due to the enhanced signal dispersion cause by the paramagnetic Ru(III) in RuHisPep, we have been able to fully assign its NMR spectrum without using isotopic labeling (Table 1). In our model complex, $a_4Ru(His)_2$, we observe paramagnetic shifts consistent with those observed previously for *cis*-(bis(imidazole))tetraammineruthenium(III), in particular histidine ϵ-protons near −27.1 ppm and His δ-protons near 3.2 ppm (*29*), suggesting that the symmetry and structure of the two complexes are similar (ie., both imidazole rings bind to Ru(III) through the same ring nitrogen). In RuHisPep, the ROESY spectrum is consistent with His 2 ϵN/His 6 δN binding. The loss of symmetry due to ϵN/δN binding and the presence of the intervening peptide

in RuHisPep appear to strongly perturb the paramagnetic field of the Ru(III). The chemical shifts of the histidine ring protons are individually (His 2 vs His 6) different, and the direction and magnitude of the paramagnetic shifts are very different from those observed in the simple inorganic complexes. As reported previously for a Ru(III) cross-linked peptide (*22*), some of the histidine ring protons do resonate near 0 ppm (see Table 1).

The paramagnetic effect of Ru(III) on the chemical shift dispersion of RuHisPep, while useful for assignment, made observation of ROE cross-peaks characteristic of α-helix difficult in many instances, due to resonance broadening. To obtain the best combination of peak sharpness and chemical shift dispersion, we had to carry out NMR experiments at 17.5 °C, resulting in some loss in helical content for RuHisPep (Figure 3b). We also were limited to a relatively short 75 ms mixing time in the ROESY experiment because longer mixing times made peaks of interest, that were broadened by the Ru(III), unobservable. Despite these experimental constraints, we do observe one weak $d_{NN}(i,i+1)$ cross-peak and one strong $d_{\alpha N}(i,i+3)$ cross-peak, as expected for helical structure. The $^3J(C_\alpha H-NH)$ coupling constants for the central alanines of RuHisPep are between 3 and 5 Hz over a broad temperature range. This range for $^3J(C_\alpha H-NH)$ is near the expected value of 3.9 Hz for an α-helix (*39*). Thus, the available NMR data point to significant population of a helical conformation for RuHisPep.

The H/D exchange data are interesting in that the observed protection factors are highest at the N-terminus and C-terminus of RuHisPep and weakest in the center. Only the protection factor for His 6 is close to the predicted value, and there is some uncertainty in this protection factor because of the overlap of the Ala 1 and His 6 amide NH resonances. In the case of Ala 7, the proximity of the ring of His 6 (A7 NH/His 6 δH cross-peak in the ROESY spectrum) likely results in steric slowing of exchange. The large protection factor of Ala 3 NH may indicate that the carbonyl of the acetyl group interacts with Ala 3 NH. Bifurcated hydrogen bonding to the amide NH's of the $i + 3$ and $i + 4$ residues by an acetyl capping group has been reported (*46*). However, a steric effect of the His 2/His 6 cross-link on the exchange of Ala 3 may also play a role in exchange protection. The faster than expected exchange for the amide NH's of Ala 4 and Ala 5 could reflect a polarizing effect of the Ru(III) that would not be accounted for in the parameters used to calculate k_{ex} for an amide NH between two alanines (*35*). Both of these amide NH's would be ~7.5 Å from the +3 charge on the metal in an α-helical conformation (based on the model studies, described above). Despite the ambiguities likely resulting from steric and polarizability effects of the ruthenium cross-link, the increase in P_{obs} for the amide NH's of Ala 4, Ala 5, and His 6 is qualitatively consistent with the predicted trend in protection factors (P_{pred}, Table 3) based on the modified Lifson−Roig model discussed in the next section.

Modification of the Lifson−Roig Helix−Coil Theory to Accommodate Nucleating Side Chain Cross-Links. Quantitative analysis of helix parameters has been carried out in a few cases where conformational constraints have been used to assist in helix nucleation (*26*, *46*). The Zimm−Bragg parameters, σ and s, have been used in these analyses and it has been assumed that $\sigma = 1$ for a prenucleated helix (*26*, *46*). The use of $\sigma = 1$ is convenient for calculations since the helix−coil partition function depends only on the value of the propagation parameter, *s*, in this case. However, the physical significance of the choice $\sigma = 1$ is less clear, since there is no restriction on σ having values >1 (*11*), except when defined in terms of the Lifson−Roig parameter, υ, where the maximal value of $\sigma = 1/16$ (*12*). The choice of $\sigma = 1$ also sets the statistical weight of the helix nucleus equal to *s* (σs with $\sigma = 1$) versus a weight of 1 for the same chain segment when in the unnucleated coil state. Given that constrained nucleation sites are assumed to lock in the helix nucleus, such relative weights for coil and nucleus would not seem to accomplish this goal, given that the maximal s weight is 1.7 (0 °C) for alanine (*7*). In the case of nucleation by a calmodulin loop, the propagation parameters of Baldwin and co-workers (*7*) had to be increased to match the observed helix content in this system. It is reasonable that prenucleation would affect both the initiation and propagation parameters in the helix−coil theory. The question is how to vary these parameters simultaneously in a rational manner.

Prenucleation in our case and in other cases (*16*−*25*, *46*) introduces a covalent constraint that restricts the ϕ,ψ angles of the protein main chain. Thus, the Lifson−Roig theory, which defines the helix parameters in terms of the ϕ,ψ space of each residue in the chain, has advantages over the Zimm−Bragg theory (which parametrizes in terms of hydrogen bonds) for approaching the problem of prenucleation with covalent constraints. In the Lifson−Roig theory, the coil state (nonhelical conformations) is taken as a reference point, and thus, the parameter, υ, is equivalent to the equilibrium constant for the coil ↔ helix transition of an individual residue (*12*). If a covalent constraint reduces the conformational space of the coil state relative to the helix state, this equilibrium should shift to the right, and υ should increase for residues constrained by the covalent cross-link. In our case, the ϕ,ψ angles of Ala 3, Ala 4, and Ala 5 are all constrained by the ruthenium cross-link between His 2 and His 6. We will assume that υ increases for all three of these residues by the same amount and define a parameter υ_{35} for these three residues to describe nucleation. The validity of assuming the same nucleation parameter for all three residues is supported by the similar $^3J(C_\alpha H-NH)$ coupling constants for Ala 3, Ala 4, and Ala 5 (Table 2), indicating that the constraints on conformational space are similar for all three. For His 2 and His 6, the side chain cross-link between these two only constrains one of the ϕ,ψ angles. For these histidines, we will assume a value for the nucleation parameter, υ_{26}, that is the geometric mean of υ_{35} and the standard nucleation parameter for an alanine-based helix, υ ($\upsilon^2 = 0.0013$, ref *7*), giving $(\upsilon_{26})^2 = \upsilon_{35} \times \upsilon$.

The Lifson−Roig theory defines statistical weights based on three conformational integrals (*12*, *13*). Using the nomenclature of Qian and Schellman (*12*), u' is the conformational integral over nonhelical conformations (coil state), where the overall weight is effectively a Boltzmann weighted sum over all conformations with respect to the conformational free energy, $W_1(i)$, of each conformation. The nucleation parameter, υ', is the same conformational integral done over helical conformations. For the propagation parameter, w', the conformational integral is also over helical angles with respect to a free energy, *W*, which is equal to the sum

of the conformational free energy, $W_1(i)$, and the interaction energy of the three consecutive helical residues, $W_3(i-1,i,i+1)$, which was presumed to be due to hydrogen bonding in the original theory. Thus, w' can be viewed as being due to a coupled equilibria and may be written as in eq 8:

$$w' = \upsilon' \times w'' \tag{8}$$

where w'' is the weighting due to $W_3(i-1,i,i+1)$. When the parameters are normalized with respect to u' to obtain the usual weights, υ, w, and 1, the parameter w can be written as in eq 9:

$$w = (\upsilon'/u') \times w'' = \upsilon \times w'' \tag{9}$$

Thus, w should increase proportionately with υ. In essence υ in eq 9 reflects the entropic contribution to w. From another perspective, as u' is decreased by a conformational constraint, the normalized parameters, υ and w, should increase by the same proportion. Therefore, the propagation parameter for the three central alanines, w_{35}, and for His 2 and His 6, w_{26}, can be written as in eqs 10 and 11, where $w_{Ala} = 1.7$ and

$$w_{35} = w_{Ala} \times (\upsilon_{35}/\upsilon) \tag{10}$$

$$w_{26} = w_{His} \times (\upsilon_{26}/\upsilon) = w_{His} \times (\upsilon_{35}/\upsilon)^{1/2} \tag{11}$$

$w_{His} = 0.36$ (0 °C), the propagation parameters reported for a standard alanine-based helix with $\upsilon^2 = 0.0013$ (*7*). Since the other amino acids, Ala 1 and Ala 7, are outside the cross-link, we assume that their conformational distributions are unaffected, and thus, the standard υ and w parameters are used for these residues (*7*). The analysis allows the helix content, f_H, of RuHisPep to be fit with one adjustable parameter, υ_{35}, and provides a rational means for scaling w when υ changes.

We fit the data in Figure 3b according to this modified Lifson−Roig theory, using the helix−coil matrix described by Rohl et al. (*7*). We use the same enthalpy, −0.8 kcal/mol, to describe the temperature dependence of all propagation parameters. This value provides a good fit for our data and is in line with other reported values for peptide helices (*41*, *47*). The nucleation parameters, υ, υ_{26}, and υ_{35}, were assumed to be temperature independent, as is usual (*12*). It is evident from the solid curve in Figure 3b that we obtain an excellent fit to the data with this model. The $[\Theta]_{222}$ versus T data appears to level off at high temperature, and this is reasonably well modeled by the curve based on the modified Lifson−Roig model (solid line Figure 3b) and eqs 3 and 4 in the Material and Methods. In fact, the fractional helicity predicted by the modified Lifson−Roig model continues to decrease. However, since the standard curves for helix and coil (eqs 3 and 4, Materials and Methods) approach each other at high temperature, the predicted ellipticity levels at low fractional helicities as temperature increases. Although there are inherent difficulties in converting between fractional helicity and $[\Theta]_{222}$ using equations such as 3 and 4 (see ref *48*), the CD data in Figure 3b, within error (see error bar in Figure 3b), is well predicted by the standard curves given by eqs 3 and 4 in conjunction with the fractional helicities predicted by the modified Lifson−Roig model presented here. Thus, use of eqs 3 and 4 is adequate for the present purposes. We also note that we have used the standard value for neutral histidine, w_{His} (*7*), to fit our data, since experimental evaluation of w for cross-linked histidines would not be straightforward. The quality of the fit to the data in Figure 3b indicates that w for cross-linked histidines is similar to w_{His}. Therefore, within error this assumption is reasonable. The best fit for the data in Figure 3b is given by a value of $(\upsilon_{35})^2 = 0.0088$. Fractional helicity, and thus $[\Theta]_{222}$, is very sensitive to the value of $(\upsilon_{35})^2$ for the fractional helicity regime of RuHisPep. In Figure 3b, long dashed lines show that the effect of changing the value of $(\upsilon_{35})^2$ by ±25%, on the temperature dependence of $[\Theta]_{222}$, is substantial. With $(\upsilon_{35})^2 = 0.0088$, the value for $(\upsilon_{26})^2$ that results is 0.0034. Thus, relatively modest 2.5−7-fold increases in υ^2 are adequate to explain the ∼15-fold increase in the helix content of the Ac-AHAAAHA-$CONH_2$ heptapeptide resulting from introduction of the $i,i+4$ Ru(III) cross-link. In terms of the shift in the coil ↔ helix equilibrium, $\upsilon_{35} = 0.094$. Thus, the cross-link is consistent with a relatively small shift in the probability of the helical state relative to the coil state. The propagation parameter, w_{35}, for alanines 3, 4, and 5 increases to 4.4 (0 °C) versus $w_{Ala} = 1.7$ (*7*), a 2.6-fold increase. The propagation parameter, w_{26}, for His 2 and His 6 increases to 0.58 (0 °C), a 1.6-fold increase. Thus, the increase in propagation parameters due to the conformational constraint is an important contributor to the enhancement of helical content of RuHisPep relative to HisPep.

To test the impact of the CD end effect (x in eq 3) on the magnitude of $(\upsilon_{35})^2$ in our modified Lifson−Roig model, we evaluated $(\upsilon_{35})^2$ with $x = 2.5$ and $x = 3.6$. We obtain values of 0.0079 and 0.0105, respectively. Thus, a reasonable value for this parameter for RuHisPep is $(\upsilon_{35})^2 = 0.009 \pm 0.002$ (for $x = 3.0 \pm 0.5$). The qualitative result is unchanged by varying x over a reasonable range; the increase in $(\upsilon_{35})^2$ relative to υ^2 is modest ∼7-fold.

If we use Qian and Schellman's relationship (*12*) between the Lifson−Roig parameter, υ, and the nucleation parameter σ in the Zimm−Bragg theory, we obtain $\sigma_{35} = 0.0063$ versus $\sigma = 0.0011$ based on Baldwin's value of $\upsilon^2 = 0.0013$ for alanine-based peptides (*7*). Thus, an ∼6-fold increase in σ is adequate to explain the enhancement in helical content in RuHisPep. Since the Lifson−Roig and Zimm−Bragg propagation parameters are essentially identical for small υ (*12*), increases in the Zimm−Bragg propagation parameter, s, in the nucleated fragment RuHisPep are important in the increase in the helix content of RuHisPep relative to HisPep. Therefore, whether using the Lifson−Roig or the Zimm−Bragg model, our analysis indicates that $i,i+4$ side chain cross-links enhance helical content by increasing both the nucleation and propagation parameters and that a relatively modest increase in the nucleation parameter is adequate to account for the substantial increases in helical content in these systems.

Recent work has suggested that $w_{Ala} = 1.7$ found by Baldwin and co-workers may be due to a context dependent stabilization by lysine of the alanine-based peptides used to develop this scale (*48*). This work indicates that the value of w_{Ala} is closer to 1.07. Since there are no lysines in our short peptide, it is possible that $w_{Ala} = 1.07$ is more appropriately used to evaluate υ_{35} in the cross-linked heptapeptide studied here. Using this value for w_{Ala}, we obtain an equally good fit of the data in Figure 3b (short dashed line) with $(\upsilon_{35})^2 = 0.0187$. Although $(\upsilon_{35})^2$ is ∼2-fold larger

using this value for w_{Ala}, qualitatively the conclusions of this analysis are the same. The increase in the nucleation parameter is modest (~15-fold) with prenucleation, and there are significant increases in the propagation parameters of the alanines ($w_{35} = 4.07$) and histidines ($w_{26} = 0.7$), within the cross-link.

To test the predictive value of our modification to the Lifson−Roig model, we have evaluated it against the data of Ghadiri and co-workers for the 17 residue peptide, Ac-AEAAAKEAAAKHAAAHA-$CONH_2$ (*22*). In the absence of a ruthenium cross-link, the reported $[\Theta]_{222}$ is −16 000 deg cm^2 dmol^{-1} at 21 °C in water at pH 6.1. This peptide is based on peptides with Glu^- and Lys^+ spaced *i*,*i*+4 reported by Marqusee and Baldwin (*49*) which are substantially stabilized at pH 7 and low salt relative to similar peptides without the glutamate side chains (*50*). Thus, a stabilizing Glu^-/Lys^+ interaction is implicated. To match the observed fractional helicity, f_H, of this peptide calculated with eqs 2−4, we must use an *i*−2,*i*+2 interaction parameter, $p_{i-2,i+2}$, of 5.15 for alanines 4 and 9 in the helix−coil matrix described by Rohl et al. (*7*) used to evaluate f_H with the Lifson−Roig helix−coil theory ($\Delta H = -0.8$ kcal/mol was used to correct propagation parameters to 21 °C, as above). When the modification to the Lifson−Roig theory described above is used to predict the effect of the *i*,*i*+4 Ru(III) cross-link on f_H for this peptide, with $\upsilon_{35} = 0.0088$ (and keeping $p_{i-2,i+2} = 5.15$ for alanines 4 and 9), we obtain $f_H = 0.82$ (at 21 °C), which corresponds to $[\Theta]_{222} = 27\,300$ deg cm^2 dmol^{-1} (21 °C). This value is very close to the experimental $[\Theta]_{222}$ of 28 000 deg cm^2 dmol^{-1} (21 °C) for this peptide when the histidines are cross-linked with Ru(III) (*22*).

CONCLUSIONS

We have demonstrated that an *i*,*i*+4 ruthenium cross-link can induce significant helical structure in a short, otherwise structureless, heptapeptide, as indicated by circular dichroism and NMR data. A modification to the Lifson−Roig model shows that the effect of the cross-link on the nucleation parameter, υ^2, is more modest than previously thought. Increases in the propagation parameter, *w*, are significant, indicating a synergy between nucleation and propagation in the effects of such cross-links on the helix content of peptides. The modification to the Lifson−Roig model is able to account for the effect of the *i*,*i*+4 cross-link on the helical content of a previously reported 17 residue peptide, indicating that it will be a useful tool in predicting the effects of prenucleation with side chain cross-links on the helix content of peptides.

REFERENCES

1. Baldwin, R. L., and Rose, G. D. (1999) Is protein folding hierarchic? I. Local structure and peptide folding, *Trends Biochem. Sci. 24*, 26−33.
2. Baldwin, R. L., and Rose, G. D. (1999) Is protein folding hierarchic? II. Folding intermediates and transition states, *Trends Biochem. Sci. 24*, 77−83.
3. Elöve, G. A., Chaffotte, A. F., Roder, H., Goldberg, M. E. (1992) Early steps in cytochrome *c* folding probed by time-resolved circular dichroism and fluorescence spectroscopy, *Biochemistry 31*, 6876−6883.
4. Kuwajima, K. (1989) The molten globule as a clue for understanding the folding cooperativity of globular-protein structure, *Proteins: Struct. Funct. Genet. 6*, 87−103.
5. Baldwin, R. L. (1995) α-Helix formation by peptides of defined sequence, *Biophys. Chem. 55*, 127−135.
6. Lacroix, E., Kortemme, T., Lopez de la Paz, M., and Serrano, L. (1999) The design of linear peptides that fold as monomeric *β*-sheet structures, *Curr. Opin. Struct. Biol. 9*, 487−493.
7. Rohl, C. A., Chakrabartty, A., and Baldwin, R. L. (1996) Helix propagation and N-cap propensities of the amino acids measured in alanine-based peptides in 40 volume percent trifluoroethanol, *Protein Sci. 5*, 2623−2627.
8. Stapley, B. J., Rohl, C. A., and Doig, A. J. (1995) Addition of side chain interactions to modified Lifson−Roig helix-coil theory: Applications to energetics of phenylalanine-methionine interactions, *Protein Sci. 4*, 2383−2391.
9. Armstrong, K. M., Fairman, R., and Baldwin, R. L. (1993) The (*i*, *i*+*4*) Phe-His interaction studied in an alanine-based α-helix, *J. Mol. Biol. 230*, 284−291.
10. Padmanabhan, S., Jimenez, M. A., Laurents, D. V., and Rico, M. (1998) Helix-stabilizing nonpolar interaction between tyrosine and leucine in aqueous and TFE solutions: 2D-^{1}H NMR and CD studies in alanine-lysine peptides, *Biochemistry 37*, 17318−17330.
11. Cantor, C. R., and Schimmel, P. R. (1980) *Biophysical Chemistry III: The Behavior of Biological Macromolecules*, Chapter 20, W. H. Freeman and Co., San Francisco.
12. Qian, H., and Schellman, J. A. (1992) Helix-coil theories: A comparative study for finite length polypeptides, *J. Phys. Chem. 96*, 3987−3994.
13. Lifson, S., and Roig, A. (1961) On the theory of helix-coil transitions in polypeptides, *J. Chem Phys. 34*, 517−528.
14. Rohl, C. A., Scholtz, J. M., York, E. J., Stewart, J. M., and Baldwin, R. L. (1992) Kinetics of amide proton exchange in helical peptides of varying chain lengths. Interpretation by the Lifson-Roig equation, *Biochemistry 31*, 1263−1269.
15. Rohl, C. A., and Baldwin, R. L. (1994) Exchange kinetics of individual amide protons in ^{15}N-labeled helical peptides, *Biochemistry 33*, 7760−7767.
16. Pease, J. H. B., Storrs, R. W., and Wemmer, D. E. (1990) Folding and activity of hybrid sequence, disulfide-stabilized peptides, *Proc. Natl. Acad. Sci. U.S.A. 87*, 5643−5647.
17. Storrs, R. W., Truckses, D., and Wemmer, D. E. (1992) Helix propagation in trifluoroethanol solutions, *Biopolymers 32*, 1695−1702.
18. Ösapay, G., and Taylor, J. W. (1992) Multicyclic polypeptide model compounds. 2. Synthesis and conformational properties of a highly α-helical uncosapeptide constrained by three side-chain to side-chain lactam bridges, *J. Am. Chem. Soc. 114*, 6966−6973.
19. Bracken, C., Gulyás, J., Taylor, J. W., and Baum, J. (1994) Synthesis and nuclear magnetic resonance structure determination of an α-helical bicyclic, lactam-bridged hexapeptide, *J. Am. Chem. Soc. 116*, 6431−6432.
20. Luo, P., Braddock, D. T., Subramanian, R. M., Meredith, S. C., Lynn, D. G. (1994) Structural and thermodynamic characterization of a bioactive peptide model of apoliprotein E: Side-chain lactam bridges to constrain the conformation, *Biochemistry 33*, 12367−12377.
21. Ghadiri, M. R., and Choi, C. (1990) Secondary structure nucleation in peptides. Transition metal ion stabilized α-helices, *J. Am. Chem. Soc. 112*, 1630−1632.
22. Ghadiri, M. R., and Fernholz, A. K. (1990) Peptide architecture. Design of stable α-helical metallopeptides via a novel exchange-inert Ru^{III} complex, *J. Am. Chem. Soc. 112*, 9633−9635.
23. Ruan, F., Chen, Y., and Hopkins, P. B. (1990) Metal ion enhanced helicity in synthetic peptides containing unnatural, metal-ligating residues, *J. Am. Chem Soc. 112*, 9403−9404.
24. Kemp, D. S., Boyd, J. G., and Muendel, C. C. (1991) The helical s constant for alanine in water derived from template-nucleated helices, *Nature 352*, 451−454.
25. Cabezas, E., and Satterthwait, A. C. (1999) The hydrogen bond mimic approach: Solid-phase synthesis of a peptide as an α-helix with a hydrazone link, *J. Am. Chem. Soc. 121*, 3862−3875.
26. Siedlecka, M., Goch, G., Ejchart, A., Sticht, H., and Bierzynski, A. (1999) α-Helix, nucleation by a calcium-binding peptide loop, *Proc. Natl. Acad. Sci. U.S.A. 96*, 903−908.
27. Pell, S. D., Sherban, M. M., Tramontano, V., and Clarke, M. J. (1989) *cis*-Tetraamminedihaloruthenium(III) halide complexes, *Inorg. Synth. 26*, 65−68.
28. Kirschner, S. (1957) Barium (ethylenediaminetetraacetato)-colbaltate(III) 4-hydrate, *Inorg. Synth. 5*, 186−188.
29. Clarke, M. J., Bailey, V. M., Doan, P. E., Hiller, C. D., LaChance-Galang, K. J., Daghlian, H., Mandal, S., Bastos, C. M., and Lang,

D. (1996) ^{1}H NMR, EPR, UV−Vis, and electrochemical studies of imidazole complexes of Ru(III). Crystal structures of *cis*-[$(Im)_2(NH_3)_4Ru^{III}$]Br_3 and [$(1MeIm)_6Ru^{II}$]$Cl_2 \cdot 2H_2O$, *Inorg. Chem. 35*, 4896−4903.

30. Kise, K. J., Jr., and Bowler, B. E. (2002) A ruthenium(II) tris-(bipyridyl) amino acid: Synthesis and direct incorporation into an α-helical peptide by solid-phase synthesis, *Inorg. Chem. 41*, 379−386.
31. Chen, G. C., and Yang, J. T. (1977) Two-point calibration of circular dichrometer with d-10-camphorsulfonic acid, *Anal. Lett. 10*, 1195−1207.
32. Rohl, C. A., and Baldwin, R. L. (1997) Comparison of NH exchange and circular dichroism as techniques for measuring the parameters of the helix-coil transition in peptides, *Biochemistry 36*, 8435−8442.
33. Luo, P., and Baldwin, R. L. (1997) Mechanism of helix induction by trifluoroethanol: A framework for extrapolating the helix-forming properties of peptides from trifluoroethanol/water mixtures back to water, *Biochemistry 36*, 8413−8421.
34. Glasoe, P. K., and Long, F. A. (1960) Use of glass electrodes to measure acidities in deuterium oxide, *J. Phys. Chem. 64*, 188−190.
35. Bai, Y., Milne, J. S., Mayne, L., and Englander, S. W. (1993) Primary structure effects on peptide group hydrogen exchange, *Proteins: Struct. Funct. Genet. 17*, 75−86.
36. Zhang, Y.-Z. (1995) Protein and peptide structure and interaction studied by hydrogen exchange and NMR, Ph.D. Thesis, Structural Biology and Molecular Biophysics, University of Pennsylvania, Philadelphia, PA.
37. Plaxco, K. W., Morton, C. J., Grimshaw, S. B., Jones, J. A., Pitkeathly, M., Campbell, I. D., and Dobson, C. M. (1997) The effects of guanidine hydrochloride on the random coil conformation and NMR chemical shifts of the peptide series GGXGG, *J. Biomol. NMR 10*, 221−230.
38. Sober, H. A. (1970) *CRC Handbook of Biochemistry*, 2nd ed., p J-119, CRC Press, Cleveland, OH.
39. Wüthrich, K. (1986) *NMR of Proteins and Nucleic Acids*, Wiley-Interscience, New York.
40. Milhauser, G. L., Stenland, C. J., Hanson, P., Bolin, K. A., and van de Ven, F. J. M. (1997) Estimating the relative population of 3_{10}-helix and α-helix in Ala-rich peptides: A hydrogen exchange and high field NMR study, *J. Mol. Biol. 267*, 963−974.
41. Lopez, M. M., Chin, D.-H., Baldwin, R. L., and Makhatadze, G. I. (2002) The enthalpy of the alanine peptide helix measured by isothermal titration calorimetry using metal-binding to induce helix formation, *Proc. Natl. Acad. Sci. U.S.A. 99*, 1298−1302.
42. Chakrabartty, A., Kortemme, S., Padmanabhan, S., and Baldwin, R. L. (1993) Aromatic side-chain contribution to far-ultraviolet circular dichroism of helical peptides and its effect on measurement of helix propensities, *Biochemistry 32*, 5560−5565.
43. Manning, M. C., and Woody, R. W. (1991) Theoretical CD studies of polypeptide helices: Examination of important electronic and geometric factors, *Biopolymers 31*, 569−586.
44. Gans, P. J., Lyu, P. C., Woody, R. W., and Kallenbach, N. R. (1991) The helix-coil transition in heterogeneous peptides with specific side chain interactions: Theory and comparison with CD spectral data, *Biopolymers 31*, 1605−1614.
45. Chakrabartty, A., Kortemme, T., and Baldwin, R. L. (1994) Helix propensities of the amino acids measured in alanine-based peptides without helix stabilizing interactions, *Protein Sci. 3*, 843−852.
46. Zhou, H. X., Hull, L. A., and Kallenbach, N. R. (1994) Quantitative evaluation of stabilizing interactions in a prenucleated α-helix by hydrogen exchange, *J. Am. Chem. Soc. 116*, 6482−6483.
47. Richardson, J. M., McMahon, K. W., MacDonald, C. C., and Makhatadze, G. I. (1999) MEARA sequence repeat of human CstF-64 polyadenylation factor is helical in solution. A spectroscopic and calorimetric study, *Biochemistry 38*, 12869−12875.
48. Williams, L., Kather, K., and Kemp, D. S. (1998) High helicities of Lys-containing, Ala-rich peptides are primarily attributable to a large context-dependent Lys stabilization, *J. Am. Chem. Soc. 120*, 11033−11043.
49. Marqusee S., and Baldwin, R. L. (1987) Helix stabilization by $Glu^- \cdots Lys^+$ salt bridges in short peptides of *de novo* design, *Proc. Natl. Acad. Sci. U.S.A. 84*, 8898−8902.
50. Marqusee, S., Robbins, V. H., and Baldwin, R. L. (1989) Unusually stable helix formation in short alanine-based peptides, *Proc. Natl. Acad. Sci., U.S.A. 86*, 5286−5290.

BI026608X